




Hydrodeoxygenation of stearic acid over Co-Mg-Al-O mixed oxide catalysts

Aleksandr Nepomniashchii* , Alina Markelova, Liudmila Buluchevskaya, Aleksandr Lavrenov 

Center of New Chemical Technologies BIC, Borekov Institute of Catalysis , Omsk 644040, Russia

* Corresponding author: himik@ihcp.ru



Abstract

The influence of the Co/Mg molar ratio on the physicochemical and catalytic properties of Co-Mg-Al-O mixed oxides obtained by thermal treatment of layered double hydroxides (LDH) was investigated. Characterization of the mixed oxides by ICP, XRD, and TPR revealed that the catalysts form solid solutions with well-dispersed cobalt particles, where increasing cobalt content weakens the interaction between Co and spinel, promoting the formation of larger Co₃O₄ crystallites and decreasing the cobalt reduction temperature. With increasing Co/Mg ratio, the conversion of stearic acid and the yield of C₁₅-C₁₈ hydrocarbons increased. The conversion of stearic acid to hydrocarbons proceeds through the formation of intermediate products—1-octadecanol and stearyl stearate—whose proportion increases with higher catalyst calcination temperature, indicating the key role of the hydrogenation metal in the conversion pathway. Complete conversion of stearic acid with heptadecane as the main product is achieved using a catalyst with a Co/Mg molar ratio of 3 at 270 °C and 4 MPa hydrogen pressure. The possibility of oxidative regeneration of this catalyst and its multi-cycle reuse was demonstrated.

Key findings

- Increasing cobalt content reduces the thermal stability of hydrotalcites and facilitates cobalt reduction from the corresponding Co-Mg-Al-O oxides under hydrogen.
- As the Co/Mg ratio increases, the stearic acid conversion and the yield of C₁₅-C₁₈ hydrocarbons increase.
- The main product of stearic acid conversion is heptadecane, formed through decarbonylation/decarboxylation reactions.
- High basicity of catalysts promotes side reactions leading to the formation of stearic acid esters.

© 2025, the Authors. This article is published in open access under the terms and conditions of the Creative Commons Attribution (CC BY) license (<http://creativecommons.org/licenses/by/4.0/>).

1. Introduction

The growing energy demand, fossil fuel depletion, and environmental issues linked to climate changes necessitate the search for new promising raw materials for energy production [1-3]. Biomass is considered one of such resources, the main advantages of which are rapid renewability, environmental friendliness and a "neutral" carbon footprint [4]. There are technologies making it possible to obtain bio-fuels from triglycerides of fatty acids (TAGs), sugar, starch or cellulose [5]. TAGs in vegetable oils and fats are particularly attractive feedstocks for motor fuel components due to their fatty acid residues with varying hydrocarbon chain lengths and low oxygen content [6]. Catalytic hydrodeoxygenation (HDO) of fat and oil sources makes it possible to

obtain hydrocarbon components of diesel fuels that meet the highest modern environmental and operational requirements. This is primarily due to the absence of oxygen-, nitrogen-, and sulfur-containing compounds, unsaturated and polycyclic aromatic hydrocarbons, as well as high cetane number [7,8]. Several industrial HDO processes are known, where oil- and fat-based feedstocks undergo hydroprocessing individually or in mixtures with petroleum fractions [9,10]. Another proposed method involves hydrolysis of TAGs to produce free fatty acids and glycerol, followed by deoxygenation of the fatty acids [11].

Palmitic, oleic, and stearic acids, the main components of TAGs, are commonly used as feedstocks for HDO [12-14]. Catalysts for HDO include metals, their oxides, or sulfides

Accompanying information

Article history

Received: 01.10.25

Revised: 05.11.25

Accepted: 05.11.25

Available online: 12.11.25

Keywords

Stearic acid; hydrodeoxygenation; cobalt; layered hydroxides; mixed oxides

Funding

This work was supported by the Russian Science Foundation (grant no. 24-23-20109, <https://rscf.ru/project/24-23-20109/>), as well as a grant in the form of a subsidy provided from the budget of the Omsk region.

Supplementary information

Supplementary materials: [▶ READ](#)

Transparent peer review: [▶ READ](#)

Sustainable Development Goals



supported on porous carriers. Three primary reaction pathways occur during HDO: hydrogenation of carboxylic acids with water elimination, yielding hydrocarbons with the same carbon count as the acid (HD), decarboxylation (deCO₂) and decarbonylation (deCO), producing hydrocarbons with one fewer carbon atom than the original acid.

Traditional hydrotreating catalysts are limited in HDO applications due to the need for sulfur-containing compounds in the feedstock to ensure process stability [15,16]. Non-sulfide catalysts based on transition metals (e.g., Ni, Co, Mo, W) are most promising for HDO of fats, oils and their derivatives due to their low cost compared to noble metals, along high activity and stability [17,18]. Nickel and cobalt catalysts are widely employed in hydrodeoxygenation (HDO) processes for «green diesel» production, where fatty alcohols serve as key intermediates. At equal metal loading, deoxygenation activity followed the order Co>Pd>Pt>Ni, with TOF values increasing as particle size increased. Ni, Pd, and Pt catalysts favored decarbonylation (DCO), whereas Co catalysts primarily exhibited decarboxylation (DCO₂) and hydrodeoxygenation (HDO) pathways [19]. Combining HDO-active components (Co or Ni) with H-ZSM-22, ZSM-5 acidity allowed direct conversion of palmitic acid to isoalkanes with 73.4% selectivity through hydroisomerization [17,20]. Zhou et al. achieved an 85.7% yield of fatty alcohol using Co/ZrO₂ by reducing reaction temperature and increasing H₂ pressure to minimize overhydrogenation [21]. Additionally, Co/Al₂O₃ catalysts have been utilized for catalytic upgrading of natural oils and derivatives to alkanes via fatty alcohol intermediates [22]. In Co/MgO system, MgO-CoO solid solution and MgCo₂O₄ spinel formation enabled high Co dispersion at low calcination temperatures and high Co loadings. During methyl heptanoate hydrogenolysis, Co/MgO's basic sites cleaved acyl C–O bonds to yield heptanal and methanol, followed by hydrogenation to 1-heptanol (55% yield). Acidic Co/SiO₂ and Co/H β cleaved ester C–O bonds to heptanoic acid and CH₄, which underwent decarbonylation/HDO to C₆/C₇ alkanes (89% total yield). These results demonstrate the critical role of metal-acid/base synergy in controlling product selectivity for vegetable oil upgrading [23].

The acid-base properties of supports significantly influence HDO of free fatty acids and TAGs. Supports with basic surface character are generally most favorable for stable HDO catalyst performance. Layered double hydroxides (LDHs), or hydrotalcite-like compounds, with the general formula $[M_{1-x}^{II}M_x^{III}(\text{OH})_2]^{x+}[A_{x/m}^{m-}] \cdot n\text{H}_2\text{O}$, where M^{II} and M^{III} represent divalent (e.g., Mg²⁺, Co²⁺, Ni²⁺) and trivalent (e.g., Al³⁺, Cr³⁺) cations, respectively, and the M^{II}/M^{III} ratio ranges from 1 to 5 [24], are of significant interest for catalytic applications. Upon calcination, these materials form mixed metal oxides and spinel-like structures exhibiting high surface area, excellent thermal stability, and composition-dependent basic properties. Furthermore, reduction of calcined samples containing reducible metal ions yields well-dispersed and thermally stable metal nanoparticles.

Studies [25,26] demonstrate the feasibility of LDH-based catalysts for biofuel production from oil- and fat-based feedstocks, achieving over 80 wt.% yield of C₈–C₁₈ hydrocarbons. Researchers [27] investigated oleic acid transformations on mixed MAO_x oxides (M = Ni, Mg, Zn, Fe) derived from LDH precursors. Mixed metal oxide phases significantly influence catalyst basicity and acidity, leading to increased hydrocarbon selectivity and yield in the order Fe<Zn<Mg<Ni. Co-based layered double hydroxides (LDHs) serve as effective precursors for high-performance catalysts, where the Co/Co⁶⁺ ratio is determined by reduction temperature. The integration of Co within the layered structure enhances redox and acid-base properties, thereby improving hydrodeoxygenation activity. In contrast to supported catalysts, whose activity declines at Co contents above 20–25 wt.% due to active site loss and surface area reduction from Co agglomeration and pore blocking, Co-containing LDHs maintain high hydrogenation component concentrations and superior Co dispersion post-reduction. Nguyen et al. [28] investigated Jatropha oil conversion using a Co-Mg-Al-O catalyst system with Mg/Al molar ratios of 0.1–1 and Co/Mg of 0.2. The resulting amorphous material exhibited a highly ordered mesoporous structure and thermal stability, achieving a diesel fraction yield of 54.3–59.4 wt.% with hydrocarbon content exceeding 70% during decarboxylation. They highlighted the positive effect of catalyst basicity and the critical role of cobalt in hydrogenation properties, supported by [29–31].

This study aims to systematically investigate the influence of Co/Mg molar ratios and pre-treatment conditions (calcination and reduction temperatures) on the structural and catalytic properties of Co-Mg-Al layered double hydroxides (LDHs) for the hydrodeoxygenation (HDO) of stearic acid. The research focuses on establishing structure-activity relationships to optimize catalyst performance, including conversion efficiency, hydrocarbon selectivity and stability.

2. Text components

2.1. Catalyst Preparation

LDHs with general formula Co_xMg_{6-x}Al₂ (x = 0, 1.5, 3, 4.5 and 6) were synthesized via co-precipitation from aqueous solutions of Co(NO₃)₂·6H₂O (Omskreaktiv, LLC, 99%), Mg(NO₃)₂·6H₂O (Omskreaktiv, LLC, 99%) and Al(NO₃)₃·9H₂O (Omskreaktiv, LLC, 99%), which were added at a temperature of 60 °C and with intensive stirring to a 2 M aqueous solution of Na₂CO₃. The precipitation pH was maintained at 10 by periodically introducing 1 M NaOH solution into the mother liquor. The nominal molar ratio (Co+Mg)/Al was fixed at 3 for all samples. The precipitate was filtered, washed with distilled water until neutral pH value, dried at 80 °C for 16 h, and calcined at 500–850 °C for 4 h. The resulting Co-Mg-Al-O mixed oxides were further treated in a hydrogen atmosphere at 500–850 °C for 2 h.

2.2. Characterizations

The chemical composition of the catalysts was determined using inductively coupled plasma atomic emission spectrometry (ICP-AES 710-ES Varian).

Thermal analysis of LDH samples was performed on a DTG-60 device (Shimadzu, Kyoto, Japan) in the temperature range of 20–850 °C under a flowing (35 ml/min) mixture of Ar and O₂ (22±1 vol.%) at a heating rate of 10 °C/min.

Phase composition was analyzed via powder X-ray diffraction (XRD) on a Bruker D8 Advance diffractometer using monochromatic Cu K α radiation ($\lambda = 1.5406 \text{ \AA}$) with a Lynxeye position-sensitive detector. The samples were scanned at room temperature over 2θ angles of 5–80° with a step size of 0.05° and a counting time of 2 sec per step (40 kV, 40 mA). The diffraction patterns were indexed using the ICDD PDF-2 powder diffraction database.

Temperature-programmable reduction (TPR) was conducted on an AutoChem II 2920 (“Micromeritics”) chemisorption analyzer equipped with a thermal conductivity detector (TCD). The sample were heated from 35–850 °C at 10 °C min in a 10 vol.% H₂/Ar mixture.

2.3. Catalytic tests

HDO of stearic acid was carried out using a stainless steel autoclave Limbo Li (Büchi Glass Uster) with a volume of 200 mL. The reactor was loaded with a catalyst (0.1 g), feedstock (2.5 g) and decane (50.0 g) as a solvent. Prior to testing, the reactor was purged with argon, followed by pressurization to 4.0 MPa with hydrogen. The reaction mixture was stirred using a mechanical stirrer at 1000 rpm. The test temperature was varied in the range of 210–270 °C with a step of 20 °C. The test duration was 5 h. Liquid products were identified using a GC-1000 gas chromatograph (Chromos) equipped with a capillary column (Restek Rtx-5, 30 m length, 0.32 mm inner diameter, 0.25 μm phase thickness) and a flame ionization detector (FID). Mass fractions of individual compounds and product groups were determined by the internal normalization method. The composition of gaseous products was analyzed using a packed column (3 m length, 4 mm diameter) filled with Porapak R sorbent in combination with a thermal conductivity detector (TCD). Qualitative composition of the products was evaluated by GC-MS (Agilent 6890N) using a capillary column (HP-5MS, 30 m length, 0.32 mm inner diameter, 0.25 μm phase thickness) and a mass spectrometer (Agilent 5973). The conversion of stearic acid (X , %) and yield (Y_i , %) of the products were calculated using equations (1) and (2), respectively:

$$X = \frac{(W_0 - W_t)}{W_0} \cdot 100\%, \quad (1)$$

$$Y_i = \frac{W_i}{W_0} \cdot 100\%, \quad (2)$$

where W_0 , W_t , and W_i are the initial content of stearic acid (wt.%), its content in the reaction medium at time t (t , h), and the content of the i^{th} component in the products, respectively.

3. Results and Discussion

3.1. Phase transformations in the Co-Mg-Al-O system

On the DTG curves (Figure 1a), three endothermic peaks (I, II, and III) are observed, corresponding to four stages of LDH structure degradation: (1) removal of physically adsorbed water (up to 150 °C), (2) elimination of interlayer water (195–210 °C), (3) dehydroxylation of brucite-like layers and (4) loss of interlayer carbonate anions (240–400 °C). Calcination at temperatures above 500 °C leads to the complete destruction of the layered structure and formation of oxide phases. The subsequent mass loss ($\Delta m = 1.8\text{--}3.0\%$) (Figure 1b) is attributed to the formation of a spinel phase [32]. The substitution of Mg²⁺ with Co²⁺ reduces the temperature of stages (3) and (4), likely due to weaker affinity of cobalt cations for carbonate anions [33–35]. Thus, the thermal stability of LDH decreases with increasing Co content.

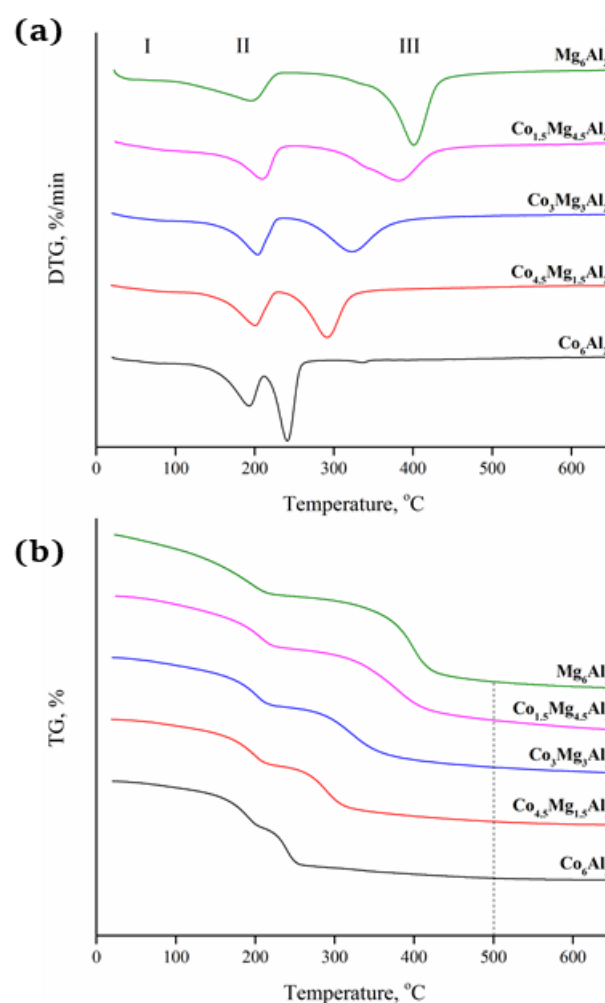


Figure 1 DTG (a) and TG (b) curves obtained during the calcination of Co_xMg_{6-x}Al₂-LDH.

Figure 2a displays XRD patterns of the LDH samples differing in the Co/Mg molar ratio. Reflections at 11.5°, 23.3°, and 34.5° indicate the preservation of the LDH structure upon cobalt incorporation [36,37]. The intensity of these reflections increases with a decrease in the Co content, suggesting enhanced crystallinity of the hydrotalcite phase, which is attributed to improved thermal stability of the samples [38,39].

The lattice parameters of hydrotalcites (HT) dried at 80°C are shown in Table 1. They indicate the presence of the hydrotalcite phase in all the dried solids. In addition, a weak diffraction peak at $2\theta = 33.45^\circ$, ascribed to cobalt hydroxide phase $\text{Co}(\text{OH})_2$, was seen only for samples containing high Co content (Co_6Al_2 and $\text{Co}_{4.5}\text{Mg}_{1.5}\text{Al}_2$). The lattice parameter *a* decreases linearly from 3.0796 Å (Co_6Al_2) to 3.0601 Å (Mg_6Al_2) with a decrease in the Co content. This is likely due to the larger ionic radius of Co^{2+} ($r = 0.74$ Å) compared to Mg^{2+} ($r = 0.65$ Å) [39], resulting in stronger electrostatic attraction between negatively and positively charged ions. Notably, the parameter *c* decreases when the $\text{Co}^{2+}/(\text{Al}^{3+} + \text{Mg}^{2+})$ ratio increases, likely due to the formation of another alternative Co-containing phase.

According to the XRD patterns of the $\text{Co}_x\text{Mg}_{6-x}\text{Al}_2$ samples calcined at 500 °C (Figure 2b), reflections corresponding to hydrotalcites are absent. This aligns with the results of thermal analysis, where complete destruction of the hydrotalcite structure was observed at this temperature. Diffraction peaks corresponding to the periclase MgO phase were detected for samples with high magnesium content. For the $\text{Co}_3\text{Mg}_3\text{Al}_2$, $\text{Co}_{4.5}\text{Mg}_{1.5}\text{Al}_2$ and Co_6Al_2 samples the observed peaks are attributed to a spinel-type structure. However, the exact nature of these oxides could not be determined definitively, as diffraction peaks corresponding to Co_3O_4 , CoAl_2O_4 and Co_2AlO_4 exhibit very similar 2θ values and intensity. The formation of Co_3O_4 is driven by the oxidation of Co^{2+} ions and the thermodynamic stability of Co_3O_4 compared to CoO under ambient conditions [45]. No diffraction peaks related to alumina phases were detected, as these phases remain in an amorphous state at the given calcination temperature.

In the XRD patterns of calcined and reduced samples at 500 °C, reflections corresponding to MgO are present (Figure 2c). Increasing Co content in reduced samples leads to a decrease in the crystallite size and an increase in the amorphous phase fraction, manifested as broadening of diffraction peaks.

Table 1 Values of the unit cell parameters for $\text{Co}_x\text{Mg}_{6-x}\text{Al}_2$ -HT solids.

Sample	a (Å)	c (Å)	d(110) (Å)
Mg_6Al_2 - HT	3.0601	23.5793	1.5301
$\text{Co}_{1.5}\text{Mg}_{4.5}\text{Al}_2$ - HT	3.0651	23.3645	1.5325
$\text{Co}_3\text{Mg}_3\text{Al}_2$ - HT	3.0689	23.2724	1.5344
$\text{Co}_{4.5}\text{Mg}_{1.5}\text{Al}_2$ - HT	3.0772	23.2775	1.5386
Co_6Al_2 - HT	3.0796	23.0286	1.5398

This is attributed to partial reduction of Co^{2+} to the metallic state. After reduction in a hydrogen stream without prior calcination, CoMgAl -HT retains part of its layered structure (Figure 2d) as skipping the oxidation in air prevents destruction of the original matrix. At high calcination temperatures, part of Co_3O_4 transforms into Co_2AlO_4 and CoAl_2O_4 , from which cobalt is reduced at higher temperatures.

For the $\text{Co}_{4.5}\text{Mg}_{1.5}\text{Al}_2$ sample, the effect of calcination temperature on the LDH structure was studied. As shown in Figure 2e, characteristic hydrotalcite diffraction peaks disappear, and new reflections at 36.8°, 44.8° and 65.2° emerge, with intensity increasing with temperature. However, it is challenging to assign these reflections to specific cobalt-based spinel phases [40]. Meanwhile, diffraction peaks of Al_2O_3 and MgO were not detected during calcination, suggesting these oxides remain amorphous or Al and/or Mg are incorporated into the Co_3O_4 lattice, forming a cobalt-based spinel structure during high-temperature treatment [41]. Given the Co/Mg ratio of 3/1, the Co_3O_4 phase is likely dominant. Additionally, a distinct CoO diffraction peak becomes evident at 850 °C, confirming the preferential formation of Co_3O_4 in calcined samples, which partially decomposes at elevated temperatures. The crystallite size calculated using the Scherrer equation for the (311) plane is approximately 73 nm, significantly larger than the 6.8 nm observed for $\text{Co}_{4.5}\text{Mg}_{1.5}\text{Al}_2$ -LDO-500.

3.2. Study of the processes occurring during the formation of the active form of the Co-Mg-Al-O catalyst

Figure 3 presents the TPR profiles of $\text{Co}_x\text{Mg}_{6-x}\text{Al}_2$ catalysts calcined at 500 °C. For the Mg_6Al_2 sample, no reduction of magnesium and aluminum oxides is observed within the studied temperature range. The TPR profiles of $\text{Co}_x\text{Mg}_{6-x}\text{Al}_2$ catalysts include two hydrogen uptake peaks: a low-temperature peak at 300–320 °C (Peak I) and high-temperature peak at 690–850 °C (Peak II). According to the XRD analysis, the calcined samples exhibit reflections corresponding to Co_3O_4 , as well as Co_2AlO_4 and/or CoAl_2O . As reported in [42], the reducibility decreases in the following order: $\text{Co}_3\text{O}_4 > \text{Co}_2\text{AlO}_4 > \text{CoAl}_2\text{O}_4$. Based on [35], Peak I can be attributed to the reduction of Co_3O_4 to CoO, followed by further reduction to metallic cobalt Co^0 . Peak II corresponds to the reduction of cobalt aluminates [43,44]. The broad, unresolved shape of this peak with shoulders suggests simultaneous reduction from multiple cobalt-containing compounds. The shift of Peak II maximum to lower temperatures with increasing cobalt content indicates easier reducibility, driven by kinetic factors, as a higher density of reactive sites accelerates the reduction rate [45].

As seen from Table 2, the experimental hydrogen consumption for $\text{Co}_{4.5}\text{Mg}_{1.5}\text{Al}_2$ and Co_6Al_2 catalysts is lower than the theoretical value required for reducing cobalt oxides to metallic Co, indicating incomplete reduction of cobalt.

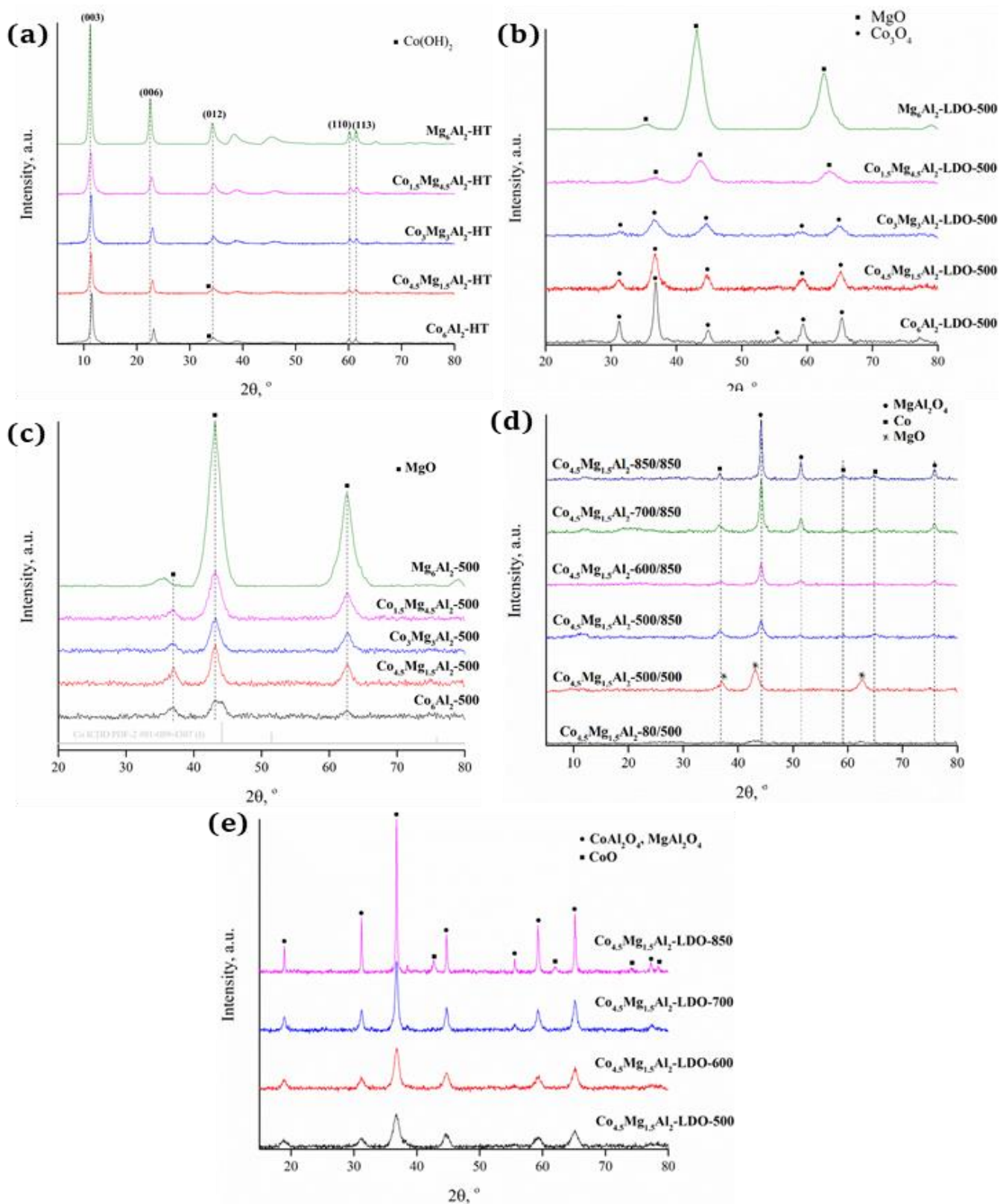


Figure 2 XRD patterns of (a) $\text{Co}_x\text{Mg}_{6-x}\text{Al}_2\text{-HT}$, (b) $\text{Co}_x\text{Mg}_{6-x}\text{Al}_2$ calcined at 500°C , (c) $\text{Co}_x\text{Mg}_{6-x}\text{Al}_2$ calcined and reduced at 500°C , (d) $\text{Co}_{4.5}\text{Mg}_{1.5}\text{Al}_2$ calcined at different temperatures and reduced at 850°C , and (e) $\text{Co}_{4.5}\text{Mg}_{1.5}\text{Al}_2$ calcined at different temperatures.

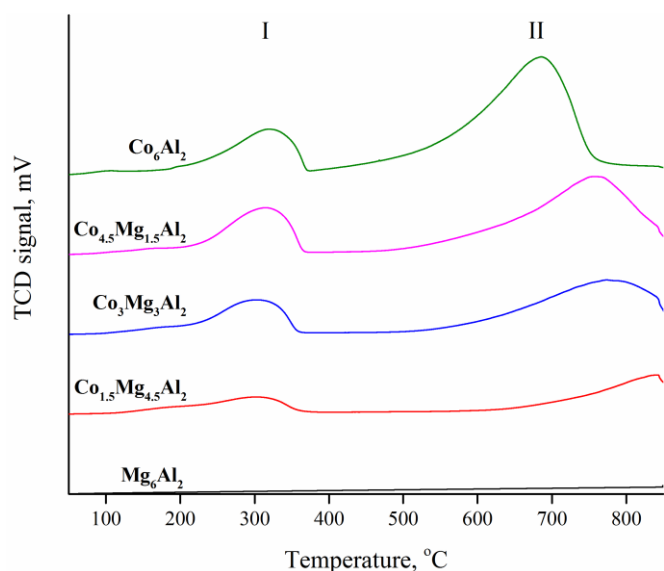


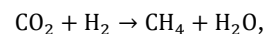
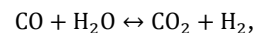
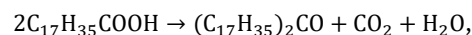
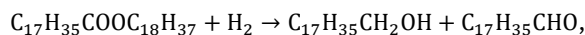
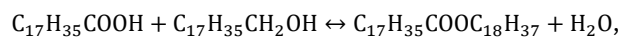
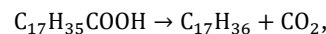
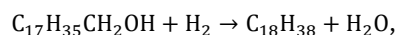
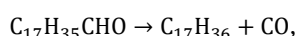
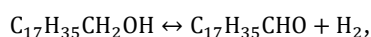
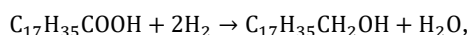
Figure 3 TPR profiles obtained for the $\text{Co}_x\text{Mg}_{6-x}\text{Al}_2$ supports calcined at 500 °C.

Table 2 Experimental and theoretical hydrogen consumption of $\text{Co}_x\text{Mg}_{6-x}\text{Al}_2$ solids calcined at 500 °C.

Sample	Co content, wt. %	H ₂ consumption [mmol H ₂ ·g ⁻¹ cat]		Theoretical H ₂ consumption [mmol H ₂ ·g ⁻¹ cat] (Co ₃ O ₄ → Co)
		I	II	
Mg ₆ Al ₂	–	–	–	–
Co _{1.5} Mg _{4.5} Al ₂	21.1	1.41	3.65	4.78
Co ₃ Mg ₃ Al ₂	37.6	2.53	6.36	8.52
Co _{4.5} Mg _{1.5} Al ₂	54.5	3.09	8.19	12.33
Co ₆ Al ₂	60.8	2.95	10.13	13.75

3.3. Investigation of the catalytic properties of Co-Mg-Al-O systems

According to the literature data [46-48], stearic acid deoxygenation proceeds via multiple pathways:



The GC-MS method identified pentadecane, hexadecane, heptadecane, octadecane, 1-octadecanol and stearyl stearate in the reaction products (Figure S1). The carbon balance of the process was calculated based on the liquid products of stearic acid conversion. When compiling the balance, the ratio between the amount of carbon in the initial feedstock and the amount of carbon in the resulting products (containing 15, 16, 17 and 18 carbon atoms) was taken into account, assuming that cracking or condensation reaction products are practically absent from the liquid or gas phases. The carbon balance for all experiments was in the range of $100 \pm 3\%$. The catalytic test results are summarized in Table 3. In the first stage, stearic acid is hydrogenated to 1-octadecanol at metallic catalyst sites [49]. Subsequent transformations of 1-octadecanol include hydrodeoxygenation (HD), removing oxygen as water, and dehydrogenation to octadecanal with decarbonylation, where oxygen is expelled as CO at metallic sites (Co) or esterification with unreacted stearic acid, catalyzed by bases [30]. The presence of C₁₅ and C₁₆ alkanes in the products arises from trace palmitic acid impurities (0.9 wt.%) in feedstock and potential hydrocracking of intermediates products at high reaction temperatures [49,50].

HDO of stearic acid at 270 °C for 5 h revealed no reaction without a catalyst. Compared to Mg₆Al₂-LDH, the conversion of stearic acid over Co_{4.5}Mg_{1.5}Al₂-LDH increased from 33.1 to 71.9%, while the yield of C₁₅-C₁₈ hydrocarbons increased from 16.3 to 20.5 wt.%.

Table 3 Evaluation of various catalysts for the catalytic hydrodeoxygenation of stearic acid ^a.

Entry	Catalyst	Conversion (%)	Yield C ₁₇ -C ₁₈ (%)	Yield alcohol (%)	C ₁₇ /C ₁₈
1 ^b	Nothing	< 1	–	–	–
2	Mg ₆ Al ₂ -LDH	33.1	16.3	0.5	11.4
3	Co _{4.5} Mg _{1.5} Al ₂ - LDH	71.9	20.5	40.2	2.1
4	Mg ₃ Al ₁ - LDO-500	27.7	15.7	1.0	13.5
5	Co _{4.5} Mg _{1.5} Al ₂ - LDO-500	60.8	10.7	33.6	6.2
6 ^c	Co _{4.5} Mg _{1.5} Al ₂ - LDH-80/500	99.9	98.5	0.1	16.4
7	Co _{4.5} Mg _{1.5} Al ₂ - LDO-500/500	100.0	98.5	0.0	13.3
8	Co ₃ Mg ₃ Al ₂ - LDO-500/500	100.0	94.4	1.2	19.6
9	Co _{1.5} Mg _{4.5} Al ₂ - LDO-500/500	50.3	4.1	22.4	2.5
10	Co ₆ Al ₂ - LDO-500/500	100.0	85.8	11.0	11.1

^a Reaction conditions: 0.1 g catalyst, 10 mmol SA, 270 °C, 5 h;

^b No catalyst was added;

^c Catalyst was reduced without prior calcination.

The main product $\text{Co}_{4.5}\text{Mg}_{1.5}\text{Al}_2\text{-LDH}$ is 1-octadecanol (40.2 wt.%), formed on Co sites acting as Lewis acid to activate the C=O bond [51]. Mixed oxides derived from calcined LDHs exhibit lower activity due to metal particle aggregation and/or non-uniform distribution, reducing accessible active sites. Magnesium in alumina-magnesia spinel participates in deoxygenation via CO_2 elimination to form MgCO_3 , which decomposes into MgO and CO_2 at high temperatures [59,60], producing C_{17} hydrocarbon. This explains the elevated $\text{C}_{17}/\text{C}_{18}$ ratio in liquid products and CO_2 detected in gases for $\text{Mg}_6\text{Al}_2\text{-LDO-500}$ (no data are provided). The absence of calcination for $\text{Co}_{4.5}\text{Mg}_{1.5}\text{Al}_2\text{-LDH-80/500}$ preserves structural and chemical advantages of LDHs, enhancing decarbonylation activity ($\text{C}_{17}/\text{C}_{18}$ ratio: 16.4).

The highest $\text{C}_{15}\text{-C}_{18}$ hydrocarbons yield (98.5%) with full stearic acid conversion was achieved using $\text{Co}_{4.5}\text{Mg}_{1.5}\text{Al}_2\text{-LDO-500/500}$. However, increasing magnesium content reduced conversion to 50.3% and hydrocarbon yield to 4.1 wt.%, with 1-octadecanol and side products detected. The reaction data indicate that stearyl stearate content in the products decreases significantly with increasing Co/Mg ratio. Since stearyl stearate conversion is directly related to catalyst hydrogenation activity, higher Co/Mg ratios enhance both hydrogenation activity and alkane yield. Selectivity for $\text{Co}_3\text{Al}_2\text{-LDO-500/500}$ decreased significantly, indicating that excess Co blocks pores and aggregates active particles, disrupting adsorption-desorption balance [52,53].

Catalyst calcination and reduction temperatures affect activity and selectivity. At full conversion, selectivity for $\text{C}_{15}\text{-C}_{18}$ hydrocarbons dropped from 98.5 to 41.5 wt.% as calcination temperature increased from 500 to 850 °C (Figure 4a). High-temperature calcination causes sintering and agglomeration of active Co particles, reducing surface area, pore volume, and acid-base site concentration involved in oxygen removal [54]. This lowers decarbonylation activity, increasing 1-octadecanol yield (20.5% → 41.7%) and ester formation.

An impact of reaction temperature on conversion and yield of main products is shown in Figure 4b. $\text{Co}_{4.5}\text{Mg}_{1.5}\text{Al}_2\text{-LDO-500/500}$ achieved full conversion at 210–270 °C. Higher temperatures increases $\text{C}_{15}\text{-C}_{18}$ yields and $\text{C}_{17}/\text{C}_{18}$ ratio via deCO and HD. Increased 1-octadecanol at lower temperatures indicates rapid hydrogenation of stearic acid to fatty alcohol, even at low temperatures, while slower HDO steps become prominent only at elevated temperatures [49]. At high temperatures $\text{C}_{15}\text{-C}_{18}$ alkanes undergo cracking to $\text{C}_5\text{-C}_{14}$ hydrocarbons and gaseous products.

3.4. Reusability and regeneration

Reusability tests on $\text{Co}_{4.5}\text{Mg}_{1.5}\text{Al}_2$ (Figure 5) showed declining activity after four cycles without regeneration: conversion dropped from 100.0% to 91.3%, and hydrocarbon yield fell from 98.5% to 80.6%.

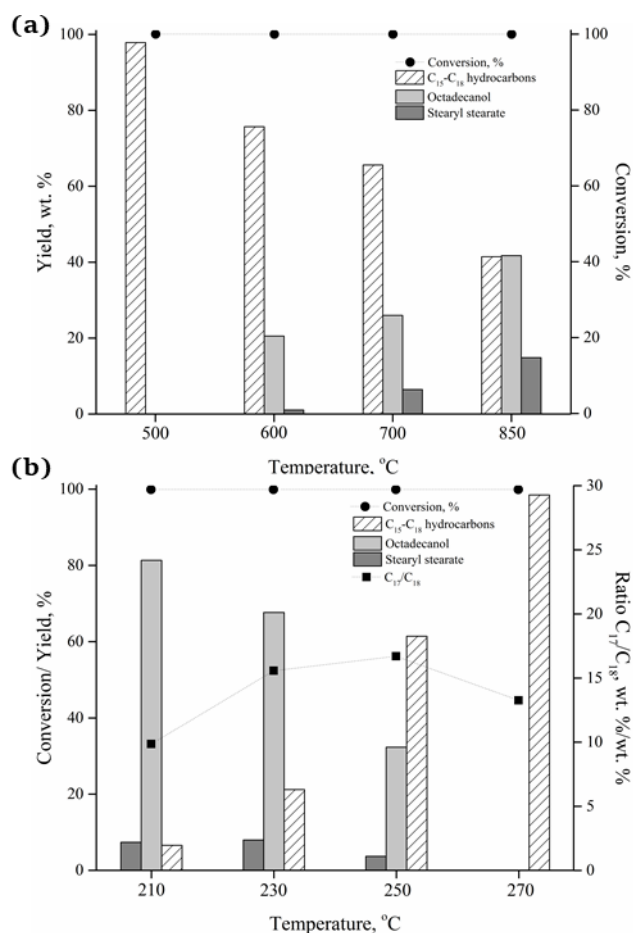


Figure 4 Influence of the calcination temperature of the catalyst (a) and the reaction temperature (b) on the conversion of stearic acid, yield and ratio of the main products in the hydrodeoxygenation process on a $\text{Co}_{4.5}\text{Mg}_{1.5}\text{Al}_2$ catalyst. (a) Reaction conditions: 0.1 g catalyst, 10 mmol SA, 270 °C, 5 h. The reduction temperature of the catalyst is 850 °C. (b) Reaction conditions: 0.1 g catalyst, 10 mmol SA, 5 h, reduction temperature of the catalyst is 500 °C.

Regeneration involved filtration, ethanol washing, drying at 120 °C, and calcination/reduction at 500 °C. No significant differences were observed between fresh and regenerated catalysts (Figure 5), demonstrating the feasibility of reusing CoMgAl mixed oxide catalysts in fatty acid hydrodeoxygenation.

In comparison with the other known catalysts that were studied in hydrodeoxygenation using a batch reactor and C_{16} or C_{18} fatty acids as feedstock (Table S1), the $\text{Co}_{4.5}\text{Mg}_{1.5}\text{Al}_2$ catalyst showed similar conversion and selectivity at a higher feed/catalyst ratio. On the other hand, it has good recyclability and good stability.

4. Limitations

This work has several limitations. Stearic acid does not account for the complex mixture of fatty acids, triglycerides, and impurities present in real biomass feedstocks. The model system lacks competitive reactions that would occur with real feedstocks. Batch experiments typically focus on short reaction times (5 h or less), which does not provide meaningful information about catalyst stability under prolonged operation.

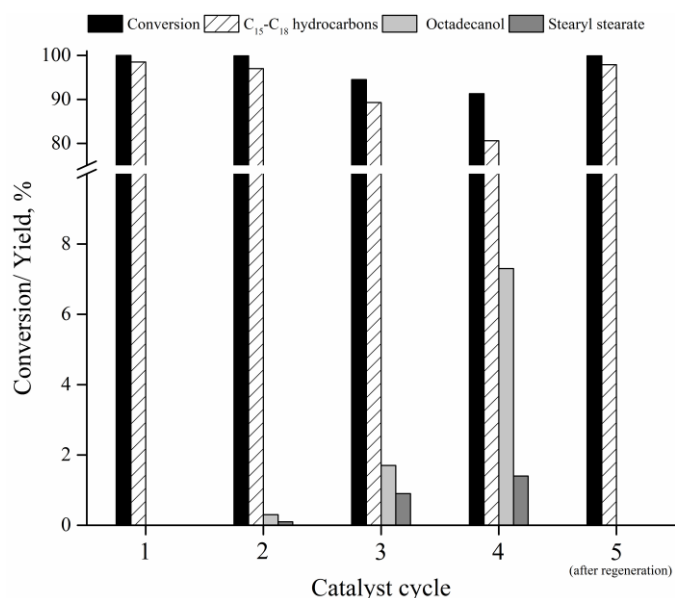


Figure 5 Reusability and regeneration of the $\text{Co}_{4.5}\text{Mg}_{1.5}\text{Al}_2$ catalyst. Reaction conditions: 0.1 g catalyst, 10 mmol stearic acid, 270 °C, 4 MPa H_2 , 5 h, 1000 rpm.

The results obtained under these experimental conditions face significant challenges in industrial application. These limitations highlight the need for complementary studies using continuous flow reactors and in-situ characterization techniques to develop a comprehensive understanding of CoMgAl catalyst performance in hydrodeoxygenation processes.

5. Conclusions

Increasing the Co/Mg ratio in CoMgAl LDHs lowers decomposition and reduction temperatures of cobalt oxides, indicating reduced thermal stability. Higher calcination temperatures cause Co particle sintering/agglomeration, hindering subsequent reduction. Hydrodeoxygenation studies on CoMgAl catalysts revealed that higher Co/Mg ratios enhance stearic acid conversion and C_{15} – C_{18} yields via decarbonylation/decarboxylation on Co metal particles and MgO-associated basic sites. At low Co content, hydrogenation to fatty alcohols and ester formation dominate.

Supplementary materials

This manuscript contains supplementary materials, which are available on the corresponding online page.

Figure S1: Gas chromatogram of liquid products from stearic acid hydrodeoxygenation; **Table S1:** The catalytic performance of $\text{Co}_{4.5}\text{Mg}_{1.5}\text{Al}_2$ compared with other reported catalysts.

Data availability statement

The data that support the findings of this study are available from the corresponding author upon reasonable request.

Acknowledgments

The authors would like to thank Kornienko N.V., Muromtsev I.V., Vasilevich A.V., Guliaeva T.I. (Center of New Chemical Technologies BIC) for their work on catalyst research. The studies were carried out using facilities of the shared research center “National

center of investigation of catalysts” at the Boreskov Institute of Catalysis.

Author contributions

Conceptualization: N.A., L.A.
Investigation: N.A., M.A., B.L.
Supervision: L.A.
Visualization: N.A.
Writing – original draft: N.A., M.A., B.L.
Writing – review & editing: N.A., L.A.

Conflict of interest

The authors declare no conflict of interest.

Additional information

Author IDs:

Alexandr Nepomniashchii, Scopus ID [57201549169](https://orcid.org/0000-0002-5720-1549);
Liudmila Buluchevskaya, Scopus ID [57213086295](https://orcid.org/0000-0002-5721-3086);
Aleksandr Lavrenov, Scopus ID [6701798395](https://orcid.org/0000-0002-6701-7983).

Website:

Boreskov Institute of Catalysis, <https://en.catalysis.ru/>.

References

- Verma D, Rana BS, Kumar R, Sibi MG, Sinha AK. Diesel and aviation kerosene with desired aromatics from hydroprocessing of jatropha oil over hydrogenation catalysts supported on hierarchical mesoporous SAPO-11. *Appl Catal A Gen.* 2015;490(1):108–116. doi:[10.1016/j.apcata.2014.11.007](https://doi.org/10.1016/j.apcata.2014.11.007)
- Alalwan HA, Alminshid AH, Aljaafari HAS. Promising evolution of biofuel generations. *Renew Energy Focus.* 2019;28:127–139. doi:[10.1016/j.ref.2018.12.006](https://doi.org/10.1016/j.ref.2018.12.006)
- Douvartzides SL, Charisiou ND, Papageridis KN, Goula MA. Green diesel: biomass feedstocks, production technologies, catalytic research, fuel properties and performance in compression ignition internal combustion engines. *Energies.* 2019;12(5):809. doi:[10.3390/en12050809](https://doi.org/10.3390/en12050809)
- Mittelbach M. Fuels from oils and fats: recent developments and perspectives. *Eur J Lipid Sci Technol.* 2015;117(11):1832–1846. doi:[10.1002/ejlt.201500125](https://doi.org/10.1002/ejlt.201500125)
- Antar M, Lyu D, Nazari M, Shah A, Zhou X, Smith DL. Biomass for a sustainable bioeconomy: an overview of world biomass production and utilization. *Renew Sustain Energy Rev.* 2021;139:110691. doi:[10.1016/j.rser.2020.110691](https://doi.org/10.1016/j.rser.2020.110691)
- Chen S, Zhou G, Miao C. Green and renewable bio-diesel produce from oil hydrodeoxygenation: Strategies for catalyst development and mechanism. *Renew Sustain Energy Rev.* 2019;101:568–589. doi:[10.1016/j.rser.2018.11.027](https://doi.org/10.1016/j.rser.2018.11.027)
- Bezergianni S, Dimitriadis A. Comparison between different types of renewable diesel. *Renew Sustain Energy Rev.* 2013;21:110–116. doi:[10.1016/j.rser.2012.12.042](https://doi.org/10.1016/j.rser.2012.12.042)
- Satyarthi JK, Chiranjeevi T, Gokak DT, Viswanathan PS. An overview of catalytic conversion of vegetable oils/fats into middle distillates. *Catalysis Sci Technol.* 2013;3(1):70–80. doi:[10.1039/C2CY20415K](https://doi.org/10.1039/C2CY20415K)
- Barbosa IV, Scapim LA, Calvante RM, Young AF. Industrial production of green diesel in Brazil: Process simulation and economic perspectives. *Renew Energy.* 2023;219:119591. doi:[10.1016/j.renene.2023.119591](https://doi.org/10.1016/j.renene.2023.119591)
- Othman MF, Adam A, Najafi G, Mamat R. Green fuel as alternative fuel for diesel engine: A review. *Renew Sustain Energy Rev.* 2017;80:694–709. doi:[10.1016/j.rser.2017.05.140](https://doi.org/10.1016/j.rser.2017.05.140)
- Mailaram S, Maity SK. Techno-economic evaluation of two alternative processes for production of green diesel from karanja oil: A pinch analysis approach. *Renew Sustain Energy Rev.* 2019;11:025906. doi:[10.1063/1.5078567](https://doi.org/10.1063/1.5078567)
- Ding S, Parlett CMA, Fan X. Recent developments in multifunctional catalysts for fatty acid hydrodeoxygenation as a

- route towards biofuels. *Mol Catal.* 2022;523:111492. doi:[10.1016/j.mcat.2021.111492](https://doi.org/10.1016/j.mcat.2021.111492)
13. Jeniřtová K, Hachemi I, Maki-Arvela P, Kumar N, Peurla M, Capek L, Warná J, Murzin DY. Hydrodeoxygenation of stearic acid and tall oil fatty acids over Nialumina catalysts: Influence of reaction parameters and kinetic modelling. *Chem Eng J.* 2017;316:401–409. doi:[10.1016/j.cej.2017.01.117](https://doi.org/10.1016/j.cej.2017.01.117)
 14. Kumar P, Yenumala SR, Maity SK, Shee D. Kinetics of hydrodeoxygenation of stearic acid using supported nickel catalysts: Effects of supports. *Appl Catal A Gen.* 2014;471:28–38. doi:[10.1016/j.apcata.2013.11.021](https://doi.org/10.1016/j.apcata.2013.11.021)
 15. Taromi AA, Kaliaguine S. Green diesel production via continuous hydrotreatment of triglycerides over mesostructured γ -alumina supported NiMo/CoMo catalysts. *Fuel Proces Technol.* 2018;171:20–30. doi:[10.1016/j.fuproc.2017.10.024](https://doi.org/10.1016/j.fuproc.2017.10.024)
 16. Wang H, Li G, Rogers K, Lin H, Zheng Y, Ng S. Hydrotreating of waste cooking oil over supported CoMoS catalyst – Catalyst deactivation mechanism study. *Mol Catal.* 2017;443:228–240. doi:[10.1016/j.mcat.2017.10.016](https://doi.org/10.1016/j.mcat.2017.10.016)
 17. Cao Y, Shi Y, Bi Y, Wu K, Hu S, Wu Y, Huang S. Hydrodeoxygenation and hydroisomerization of palmitic acid over bi-functional Co/H-ZSM-22 catalysts. *Fuel Proces Technol.* 2018;172:29–35. doi:[10.1016/j.fuproc.2017.09.020](https://doi.org/10.1016/j.fuproc.2017.09.020)
 18. Zhang H, Lin H, Zheng Y. The role of cobalt and nickel in deoxygenation of vegetable oils. *Appl Catal B Environ.* 2014;160:415–422. doi:[10.1016/j.apcatb.2014.05.043](https://doi.org/10.1016/j.apcatb.2014.05.043)
 19. Srifa A, Faungnawakij K, Itthibenchapong V, Assabumrungrat S. Roles of monometallic catalysts in hydrodeoxygenation of palm oil to green diesel *Chem Eng J.* 2015;278:249–258. doi:[10.1016/j.cej.2014.09.106](https://doi.org/10.1016/j.cej.2014.09.106)
 20. Ojeda M, Osterman N, Dražić G, Žilnik LF, Meden A, Kwapiński W, Balu AM, Likozar B, Tušar NN. Conversion of Palmitic Acid Over Bi-functional Ni/ZSM-5 Catalyst: Effect of Stoichiometric Ni/Al Molar Ratio. *Top Catal.* 2018;61:1757–1768. doi:[10.1007/s11244-018-1046-7](https://doi.org/10.1007/s11244-018-1046-7)
 21. Zhou Y, Liu X, Yu P, Hu C. Temperature-tuned selectivity to alkanes or alcohol from ethyl palmitate deoxygenation over zirconia-supported cobalt catalyst. *Fuel.* 2020;278:118295. doi:[10.1016/j.fuel.2020.118295](https://doi.org/10.1016/j.fuel.2020.118295)
 22. Arun N, Sharma RV, Dalai AK. *Renew Sustain Energy Rev.* 2015;48:240–255. doi:[10.1016/j.rser.2015.03.07421](https://doi.org/10.1016/j.rser.2015.03.07421)
 23. Li Q, Bie Y, Qiu S, Zhang Q, Sainio J, Wang T, Ma L, Lehtonen J. Hydrogenolysis of methyl heptanoate over Co based catalysts: Mediation of support property on activity and product distribution. *Appl Catal B Environ.* 2014;147:236–245. doi:[10.1016/j.apcatb.2013.08.045](https://doi.org/10.1016/j.apcatb.2013.08.045)
 24. Wang P, Zhang XQ, Zhou B, Meng FP, Wang YH, Wen GW. Recent advance of layered double hydroxides materials: structure, properties, synthesis, modification and applications of wastewater treatment. *J Environ Chem Eng.* 2023;11:111191. doi:[10.1016/j.jece.2023.111191](https://doi.org/10.1016/j.jece.2023.111191)
 25. Romero M, Pizzi A, Toscano G, Bosio B, Arato E. Study of an innovative process for the production of biofuels using non-edible vegetable oils. *Chem Eng J.* 2014;37:883–888. doi:[10.3303/CET1437148](https://doi.org/10.3303/CET1437148)
 26. Patil SJ, Vaidya PD. On the production of bio-hydrogenated diesel over hydrotalcite-like supported palladium and ruthenium catalysts. *Fuel Proces Technol.* 2018;169:142–149. doi:[10.1016/j.fuproc.2017.09.026](https://doi.org/10.1016/j.fuproc.2017.09.026)
 27. Abidin S, Lee H, Mijan N, Juan JC, Rahman N, Mastuli MS, Taufiq-Yap YH, Kong PS. Ni, Zn and Fe hydrotalcite-like catalysts for catalytic biomass compound into green biofuel. *Pure Appl Chem.* 2020;92(4):587–600. doi:[10.1515/pac-2019-0820](https://doi.org/10.1515/pac-2019-0820)
 28. Nguyen HKD, Nguyen HV, Dao DS, Hoang LL. Preparation and characterization of ordered mesoporous Mg–Al–Co hydrotalcite based catalyst for decarboxylation of jatropha oil. *J Porous Mater.* 2017;24:731–740. doi:[10.1007/s10934-016-0310-0](https://doi.org/10.1007/s10934-016-0310-0)
 29. Goulas KA, Mironenko AV, Jenness GR, Mazal T. Vlachos DG. Fundamentals of C–O bond activation on metal oxide catalysts. *Nat Catal.* 2019;2:269–276. doi:[10.1038/s41929-019-0234-6](https://doi.org/10.1038/s41929-019-0234-6)
 30. Žula M, Grilc M, Likozar B. Hydrocracking, hydrogenation and hydro-deoxygenation of fatty acids, esters and glycerides: mechanisms, kinetics and transport phenomena. *Chem Eng J.* 2022;444:136564. doi:[10.1016/j.cej.2022.136564](https://doi.org/10.1016/j.cej.2022.136564)
 31. Cheah KW, Yusup S, Loy ACM, How BS, Skoulou V, Taylor MJ. Recent advances in the catalytic deoxygenation of plant oils and prototypical fatty acid models compounds: catalysis, process, and kinetics. *Mol Catal.* 2022;523:111469. doi:[10.1016/j.mcat.2021.111469](https://doi.org/10.1016/j.mcat.2021.111469)
 32. Frolich K, Kocík J, Mück J, Kolena J, Skuhrovcová L. The role of Zn in the CuZn–Al mixed oxide catalyst and its effect on glycerol hydrogenolysis. *Mol Catal.* 2022;533:112796. doi:[10.1016/j.mcat.2022.112796](https://doi.org/10.1016/j.mcat.2022.112796)
 33. Issa S. Production of hydrogen by dry reforming of methane in the presence of mixed oxides Co–Mg–Al–O and the effect of adding Ru on the catalytic properties of these oxides; 2009; Balamand: University of Balamand, Lebanon.
 34. Vaccari A, Gazzano M. Hydrotalcite-type anionic clays as precursors of highsurface-area Ni/Mg/Al mixed oxides. *Stud Surf Sci Catal.* 1995;91:893–902. doi:[10.1016/S0167-2991\(06\)81832-X](https://doi.org/10.1016/S0167-2991(06)81832-X)
 35. Ribet S, Tichit D, Coq B, Ducourant B, Morato F. Synthesis and activation of CoMg–Al layered double hydroxides. *J Solid State Chem.* 1999;142:382–392. doi:[10.1006/jssc.1998.8053](https://doi.org/10.1006/jssc.1998.8053)
 36. Kobzar EO, Stepanova LN, Nepomniashchii AA, Vasilevich AV, Gulyaeva TI, Trenikhin MV, Lavrenov AV. CuCoMgAlOx Mixed Oxides as Selective Catalysts for the Hydrogenation of Furan Compounds. *Hydrogen.* 2023;4:644–657. doi:[10.3390/hydrogen4030041](https://doi.org/10.3390/hydrogen4030041)
 37. Li N, Xing X, Sun YG, Cheng J, Wan G, Zhang ZS, Hao ZP. Catalytic oxidation of o-chlorophenol over Co₂XAl (X = Co, Mg, Ca, Ni) hydrotalcite-derived mixed oxide catalysts. *Front Environ Sci Eng.* 2020;14:105–161. doi:[10.1007/s11783-020-1284-3](https://doi.org/10.1007/s11783-020-1284-3)
 38. Gennequin C, Kouassi S, Tidahy L, Cousin R, Lamonier J-F, Garcon G, Shirali P, Cazier F, Aboukaïs A, Siffert S. Co–Mg–Al oxides issued of hydrotalcite precursors for total oxidation of volatile organic compounds. Identification and toxicological impact of the by-products. *C R Chim.* 2010;13:494–501. doi:[10.1016/j.crci.2010.01.001](https://doi.org/10.1016/j.crci.2010.01.001)
 39. Dou LG, Fan T, Zhang H, A novel 3D oxide nanosheet array catalyst derived from hierarchical structured array-like CoMgAl–LDH/graphene nanohybrid for highly efficient NOx capture and catalytic soot combustion. *Catal Sci Technol.* 2015;5:5153–5167. doi:[10.1039/C5CY00846H](https://doi.org/10.1039/C5CY00846H)
 40. Qin LZ, Lu WMZ, Wu Z, Zhou WY. Catalyst performance of the calcined products of CoAl layered double hydroxide in the aerobic oxidation of ethylbenzene. *Catal Lett.* 2023;153:1818–1825. doi:[10.1007/s10562-022-04117-w](https://doi.org/10.1007/s10562-022-04117-w)
 41. Li Q, Meng M, Tsubaki N, Li XG, Li ZQ, Xie YN, Hu TD, Zhang J. Performance of K-promoted hydrotalcite-derived CoMgAlO catalysts used for soot combustion, NOx storage and simultaneous soot–NO_x removal. *Appl Catal B Environ.* 2009;91(1–2):406–415. doi:[10.1016/j.apcatb.2009.06.007](https://doi.org/10.1016/j.apcatb.2009.06.007)
 42. Wang HY, Ruckenstein E. Conversion of methane to syngas over Co/Al₂O₃. *Catal Lett.* 2001;75:13–18. doi:[10.1023/A:1016719703118](https://doi.org/10.1023/A:1016719703118)
 43. Gennequin C, Barakat T, Tidahy HL, Cousin R, Lamonier J-F, Aboukaïs A, Siffert S, Use and observation of the hydrotalcite «memory effect» for VOC oxidation. *Catal Today.* 2010;157:191–197. doi:[10.1016/j.cattod.2010.03.012](https://doi.org/10.1016/j.cattod.2010.03.012)
 44. Wang Z, Jiang Z, Shangguan W. Simultaneous catalytic removal of NOx and soot particulate over Co–Al mixed oxide catalysts derived from hydrotalcites. *Catal Commun.* 2007;8:1659–1664. doi:[10.1016/j.catcom.2007.01.025](https://doi.org/10.1016/j.catcom.2007.01.025)
 45. Aoun A, Aouad S, El-Khoury B, El-Nakat H, Abi-Aad E, Aboukaïs A. Catalytic oxidation of carbon black over Ru/Mgx–CoyAlz catalysts. *Phys Procedia.* 2011;21:1–5. doi:[10.1016/j.phpro.2011.10.001](https://doi.org/10.1016/j.phpro.2011.10.001)
 46. Kubickova I, Snare M, Eranen K, Maki-Arvela P, Murzin DY. Hydrocarbons for diesel fuel via decarboxylation of vegetable

- oils. *Catal Today*. 2005;106:197–200. doi:[10.1016/j.cattod.2005.07.188](https://doi.org/10.1016/j.cattod.2005.07.188)
47. Snare M, Kubickova I, Maki-Arvela P, Eranen K, Murzin DYU. Heterogeneous Catalytic Deoxygenation of Stearic Acid for Production of Biodiesel. *Ind Eng Chem Res*. 2006;45:5708–5715. doi:[10.1021/ie060334i](https://doi.org/10.1021/ie060334i)
48. Do PT, Chiappero M, Lobban LL, Resasco DE. Catalytic Deoxygenation of Methyl-Octanoate and Methyl-Stearate on Pt/Al₂O₃. *Catal Lett*. 2009;130:9–18. doi:[10.1007/s10562-009-9900-7](https://doi.org/10.1007/s10562-009-9900-7)
49. Kumar P, Maity SK, Shee D. Hydrodeoxygenation of stearic acid to produce green diesel over alumina supported CoMo catalysts: Role of Co/Mo mole ratio. *Renew Energy*. 2024;237:121700. doi:[10.1016/j.renene.2024.121700](https://doi.org/10.1016/j.renene.2024.121700)
50. Kumar P, Maity SK, Shee D. Role of NiMo alloy and Ni species in the performance of NiMo/Alumina catalysts for hydrodeoxygenation of stearic acid: A kinetic study. *JACS Omega*. 2019;4:2833–2843. doi:[10.1021/acsomega.8b03592](https://doi.org/10.1021/acsomega.8b03592)
51. Cheng S, Ding J, Chen Y, Pan G, Feng X, Xu X, Xu J. Enhanced catalytic transfer hydrogenation of biomass-based furfural into furfuryl alcohol over Co₃O₄-based mixed oxide catalysts from hydrotalcite. *App Catal A Gen*. 2024;684:119909. doi:[10.1016/j.apcata.2024.119909](https://doi.org/10.1016/j.apcata.2024.119909)
52. Zhang A, Ma Q, Wang K, Liu X, Shuler P, Tang Y. Naphthenic acid removal from crude oil through catalytic decarboxylation on magnesium oxide. *Appl Catal A Gen*. 2006;303:103–109. doi:[10.1016/j.apcata.2006.01.038](https://doi.org/10.1016/j.apcata.2006.01.038)
53. Morgan T, Santillan-Jimenez E, Harman-Ware AE, Ji Y, Grubb D, Crocker M. Catalytic deoxygenation of triglycerides over supported nickel catalysts. *Chem Eng J*. 2012;189:346–355. doi:[10.1016/j.fuel.2012.08.035](https://doi.org/10.1016/j.fuel.2012.08.035)
54. Espitia-Sibaja M, Muñoz M. Effects of the cobalt content of catalysts prepared from hydrotalcites synthesized by ultrasound-assisted coprecipitation on hydrogen production by oxidative steam reforming of ethanol (OSRE). *Fuel*. 2017;194:7–16. doi:[10.1016/j.fuel.2016.12.086](https://doi.org/10.1016/j.fuel.2016.12.086)